Available online at BCREC website: https://bcrec.id

Bulletin of Chemical Reaction Engineering & Catalysis, 18 (4) 2023, 675-687

Research Article

Catalytic Dry-reforming of Methane Process with Co,Ni,Pd/Ca-La-O Mixed Oxides

Faris A.J. Al-Doghachi[1,2,*], Ali M.A. Al-Najar[1], M. Safa-Gamal[2], Yun Hin Taufiq-Yap[2,3,*]

[1]Department of Chemistry, Faculty of Science, University of Basra, 61004, Basra, Iraq.
[2]Catalysis Science and Technology Research Centre, Faculty of Science, University Putra Malaysia, 43400, UPM Serdang, Selangor, Malaysia.
[3]Institute of Plantation Studies, Universiti Putra Malaysia, 43400, UPM Serdang, Selangor, Malaysia.

Received: 13th October 2023; Revised: 20th November 2023; Accepted: 21st November 2023
Available online: 24th November 2023; Published regularly: December 2023

Abstract

A surfactant-assisted co-precipitation method was used to prepare the catalysts Co,Ni,Pd/CaO, Co,Ni,Pd/$Ca_{0.97}La^{3+}_{0.03}O$, Co,Ni,Pd/$Ca_{0.93}La^{3+}_{0.07}O$, and Co,Ni,Pd/$Ca_{0.85}La^{3+}_{0.15}O$ (1% each of Co, Ni, and Pd). La_2O_3 doping effect on the activity and stability of Co,Ni,Pd/CaO catalysts was investigated in dry reforming of methane. Catalysts were characterized by several techniques (X-ray diffraction (XRD), Brunauer–Emmett–Teller (BET), X-ray Fluorescence (XRF), Fourier Transform Infra Red (FTIR), Temperature Programmed Desorption H_2 (H_2-TPR), Transmission electron microscopes (TEM), and Temperature Gravimetric Analysis (TGA)) and were tested in a fixed-bed reactor at 900 °C and (Gas Hourly Specific Velocity (GHSV) = 15000 $mL.g_{cat}^{-1}.h^{-1}$, atmospheric pressure). Adding La_2O_3 had little effect on the morphology of the Co,Ni,Pd/CaO catalyst. However, it played a crucial role in enhancing the catalyst's reducibility and CO_2 adsorption at high temperatures, as indicated by the activity and stability of the Co,Ni,Pd/CaO catalyst. The carbon deposition on utilized catalysts after 5 hours at 900 °C was examined using TEM and thermal gravimetric analysis (TGA) techniques. Compared to Co,Ni,Pd/CaO catalysts across the entire temperature range, the tri-metallic Co,Ni,Pd/$Ca_{0.85}La^{3+}_{0.15}O$ catalyst with a lanthanum promoter demonstrated a greater conversion of CH_4 (84%) and CO_2 (92 %) at a 1:1 CH_4:CO_2 ratio. The selectivity of H_2/CO reduced in the following order: Co,Ni,Pd/$Ca_{0.85}La^{3+}_{0.15}O$ > Co,Ni,Pd/$Ca_{0.93}La^{3+}_{0.07}O$ > Co,Ni,Pd/$Ca_{0.97}La^{3+}_{0.03}O$ > Co,Ni,Pd/CaO.

Keywords: Biogas; Dry reforming; Catalyst deactivation; Syngas; H_2 production

How to Cite: Al-Doghachi, F.J., Al-Najar, A.M.A., Safa-Gamal, M., Taufiq-Yap, Y.H. (2023). Catalytic Dry-reforming of Methane Process with Co,Ni,Pd/Ca-La-O Mixed Oxides. *Bulletin of Chemical Reaction Engineering & Catalysis*, 18(4), 675-687 (doi: 10.9767/bcrec.20053)

Permalink/DOI: https://doi.org/10.9767/bcrec.20053

1. Introduction

In recent years, global warming has been the most challenging aspect of our environment due to the permanent increase in the emission of greenhouse gases. Thus, reducing the emission of these gases by developing innovative processes capable of converting such products to useful chemicals is of prime concern worldwide. One of the solutions proposed is the utilization of the Dry Reforming of Methane (DRM) reaction (Equation (1)) to produce syngas (CO and H_2), a process extensively investigated in the last few decades [1,2]. Compared to the steam reforming reaction (Equation (2)) [3], the DRM reaction produces syngas with a lower H_2/CO ratio (*i.e.*, 1.0) [4,5], which is appropriate for the Fischer-Tropsch and methanol syntheses [5]. Hence, the DRM reaction can lower two greenhouse gases,

* Corresponding Author.
Email: farisj63@gmail.com (F.A.J. Al-Doghachi)
taufiq@upm.edu.my (Y.H. Taufiq-Yap)

making it an attractive and environmentally friendly process [6]. Unfortunately, no extensive industry application of this process has been achieved mainly due to the severe deactivation of catalysts, mostly caused by the sintering of the nickel particle (active phase) and the deposition of filamentous carbon that leads to the reactor blockage [2]. The carbon formations on the active catalytic surface are mainly attributed to the Boudouard's reaction (Equation (3)) and methane decomposition (Equation (4)).

$$CH_4 + CO_2 \rightarrow 2CO + 2H_2 \quad (1)$$
$$\Delta H_{298\,K} = +247 \text{ kJ.mol}^{-1}$$
$$CH_4 + H_2O \rightarrow CO + 3H_2 \quad (2)$$
$$\Delta H_{298\,K} = +206 \text{ kJ.mol}^{-1}$$
$$2CO \rightarrow CO_2 + C \quad (3)$$
$$\Delta H_{298\,K} = -173 \text{ kJ.mol}^{-1}$$
$$CH_4 \rightarrow C_{(S)} + 2H_2 \quad (4)$$
$$\Delta H_{298\,K} = +75 \text{ kJ.mol}^{-1}$$

According to the literature, the DRM reaction has been investigated over different materials such as exchanged zeolites [7], mixed oxides such as Al_2O_3, CeO_2, La_2O_3, *etc.* [8,9], and supported noble metal catalysts (e.g., Ru, Rh, and Pt) with high stability and activity and less sensitivity to coke formation [10,11]. The major drawback when using noble materials is their high cost and limited availability, which markedly limit their applications on a large scale. Other cheaper transition metals, such as Ni and Co, have been extensively investigated as catalysts for DRM [12]. Nevertheless, their rapid deactivation by coke deposition and sintering of the metallic phase is still a drawback for industrial implementation despite the innovative approaches developed to overcome these limitations [13–15]. To overcome this drawback, alternative options have been undertaken. In the case of Ni, the size of metallic particles is crucial, as it controls the catalytic activity behaviour. In this context, it has been found that small Ni particles inhibit coke formation [16].

An innovative way to increase the metal dispersion on the catalysts is to introduce the active phase in a well-defined structure, for instance, in hydrotalcite-based structures. Hydrotalcite (HT)-type compounds are anionic clays called layered double hydroxides (LDH). The structure is based on a mixture of divalent and trivalent metal cations randomly occupying the centers of coplanar edge sharing $M(OH)_6$ octahedral and forming sheets similar to those in the brucite structure, $[M_{1-x}^{2+} M_x^{3+} (OH)_2]x^+[A_{n-x}/n].m\ H_2O$ is the general formula of hydrotalcite (HT) where M^{2+}, M^{3+} are the divalent and trivalent metals occupying octahedral positions, the ions (CO_3^{2-}, NO_3^-, Cl^-, OH^-) are the inter-layer anions or organic anions with n charge; x and m are the fraction constants [17], respectively. The alkaline anionic clay type hydrotalcite is widely used as a catalyst with minimal carbon formation due to its fundamental properties, as well as the cations (Ni^{2+}, Mg^{2+}, Co^{2+}, Al^{3+}, Ce^{3+}, La^{3+}, *etc.*), being homogeneously distributed within the brucite type sheets. Their low density and high surface area characterize this new class of materials. The influence of thermal decomposition on these materials' stability and catalytic activity has been widely investigated [17].

This study aimed to prepare a catalyst with high activity, stability, and ability to prevent carbon deposition on the catalyst during the dry reforming of the methane reaction. The $Co,Ni,Pd/Ca_{1-x}La^{3+}{}_xO$ catalysts were prepared by using the co-precipitation method with K_2CO_3 as a precipitant, followed by the impregnation of 1% of Co, Ni, and Pd using $Co(acac)_2$, $Ni(acac)_2$, and $Pd(acac)_2$, respectively. The catalytic stability and coke formation were then compared and the effects of the concentrations of CO_2 and CH_4, the concentration of the catalysts, and the temperature of the conversion of the catalytic performance of the prepared catalysts in the dry reforming process, Finally, the study evaluated the stability of the catalyst.

2. Materials and Methods

2.1 Materials

$La(NO_3)_3.6H_2O$ (99.0%), $Ca(NO_3)_2.6H_2O$ (99.0%) and K_2CO_3 (99.7%) were obtained from Merck Company. $Co(C_5H_7O_2)_2.H_2O$ (99.0%) and $Ni(C_5H_7O_2)_2.H_2O$ (99.0%) were provided by Acros Chemicals Company. $Pd(C_5H_7O_2)_2.H_2O$ (99.5%) was obtained from Sigma-Aldrich company.

2.2 Methods

2.2.1. Preparation of catalysts

This section focuses on the preparation of the catalyst to investigate the impact of varying $Ca_{1-x}La_xO$ compositions (x = 0.00, 0.03, 0.07 and 0.15), using the co-precipitation method. It was found that La_2O_3 promoted CaO and its synthesis followed the procedure outlined in the literature [18]. The composition is expressed in mol percentage, ensuring precise control over the molar ratios of the constituent elements during the catalyst preparation. Using (0.1 M) $La(NO_3)_3.6H_2O$, $Ca(NO_3)_2.6H_2O$, and (1.0 M) K_2CO_3. Table 1 illustrates the volume used in the precipitator (K_2CO_3). Filtra-

tion was employed to collect the filtrate, which was washed with hot water and then dried at 120 °C for 12 h. The filtrate was then calcined in air at 500 °C for 5 h. to eliminate unwanted carbon dioxide and the sample was pressed to form tablets at a speed of 600 kg/m². Finally, calcine was carried out at 1150 °C for 20 h to enhance chemical properties and ensure a smooth interaction of CaO and La_2O_3. Table 1 lists the steps required to prepare catalyst concentrations of Co, Pd, and Ni(acac)$_2$/$Ca_{1-x}La_xO$ (1%) from individual Co, Pd, and Ni minerals. The first Co $(C_5H_7O_2)_2.H_2O$ was used to impregnate 1% Co dissolved in dichloromethane for 5 h. to produce Co (acac)$_2$/$Ca_{1-x}La_xO$. The catalyst was then impregnated with (1%) Pd and Ni by stirring with $Pd(C_5H_7O_2)_2.H_2O$ and $Ni(C_5H_7O_2)_2.H_2O$ in dichloromethane solutions for 5 h. After impregnation in the air, the obtained catalysts were dried at 120 °C 12 h, crushed and sieved into particles of sizes 80-150 or 150-250 μm in diameter.

2.2.2 Characterization of the catalysts

For the characterization of catalysts, various analytical techniques were employed. A diffractometer was adopted for these studies to get an idea of the crystal of the sample (Shimadzu model XRD 6000). The radiation was emitted from a Philips glass diffraction X-ray tube of broad focus 2.7 kW. The scanning range was set from 2θ = 10–80° with a scan speed of 2 °/min. Debye-Scherrer's equation is utilized to calculate the size of crystals [19]. The Kratos Axis Ultra DLD system is measured with a monochromatic Al-Kα (1486.6 eV) and two X-ray sources (Al & Ca). A catalyst temperature-programmed Reduction (H_2-TPR) method was used to determine the active sites that required hydrogen for working. The apparatus used to determine the parameters was obtained from Thermo Finnegan TPDRO 1100, accompanied by a thermal conductivity detector. Fourier transform infrared (FTIR) analysis was performed using the Agilent Cary 630 FTIR at ambient temperature to identify the chemical functional groups of the catalysts. The spectrometer resolution was set at 4 cm^{-1}, covering a range from 370 to 4000 cm^{-1}. The Thermo Fisher Scientific S.P.A Surface Analyzer, model Nitrogen adsorption-desorption, was utilized to assess the surface area through the Brunauer-Emmett-Teller (BET) method, employing low-temperature nitrogen physisorption isotherms, with nitrogen flow gas for adsorption was set at −196 °C. Transmission Electron Microscopy (TEM) (Hitachi H7100 TEM with an increasing voltage of 10 MV) was used to investigate the crystal system type and the catalyst's homogeneity. Thermogravimetric analysis (TGA) was conducted using a Mettler Toledo TG-DTA apparatus under a nitrogen atmosphere, with a flow rate of 50 $mL.min^{-1}$ and a temperature range of 50 to 1000 °C at a heating rate of 5 $°C.min^{-1}$. This method evaluated the thermal stability of the catalyst by examining its weight loss with increasing heating rates.

2.2.3 Catalytic evaluations

The synthesis gas (H_2/CO) as a sample for the reforming of biogas was conducted using a fixed bed stainless steel micro-reactor (i.d. Ø = 6 mm, h = 34 cm) through the catalytic assessment for DRM. Secondly, a mass flow gas controller (SIERRA instrument) and an online gas chromatography (GC) (Agilent 6890N; G 1540N) provided with Varian capillary columns HPPLOT/Q and HP-MOLSIV were attached to a reactor. Before the launch of the process, the cut-down of approximately 0.02 g of the catalyst was conducted by flowing 5% H_2/Ar at 700 °C, and holding for 3 h. The main objective of the reduction process was to convert the (Ni^{2+}, Pd^{2+}, and Co^{2+}) phase of the catalyst to the metal (Ni°, Pd°, and Co°) phase on the active sites of the catalyst. The examined catalysts were kept vertical using the block of quartz wool in the middle of a reactor. A thermocouple was put into the catalyst room to control and test the reaction temperature. Finally, the conversions for CH_4 and CO_2, selectivity for H_2

Table 1. Concentrations required for preparing the catalyst Co,Ni,Pd(acac)$_2$/$Ca_{1-x}La_xO$.

Catalysts	Support (CaO) $Ca(NO_3)_2.6H_2O$ (g)	Promoter (La_2O_3) $La(NO_3)_3.6H_2O$ (g)	Total weight of CaO and La_2O_3 after calcining (g)	Impregnation of the main catalyst (1% Co) (1% Pd) (1% Ni) (g)		
				$Pd(acac)_2$	$Co(acac)_2$	$Ni(acac)_2$
Co,Ni,Pd/CaO	24.0	0.0	1	0.028	0.044	0.044
Co,Ni,Pd/$Ca_{0.97}La^{+3}_{0.03}O$	22.9	1.3	1	0.028	0. 044	0.044
Co,Ni,Pd/$Ca_{0.93}La^{+3}_{0.07}O$	22.5	3.0	1	0.028	0. 044	0.044
Co,Ni,Pd/$Ca_{0.85}La^{+3}_{0.15}O$	20.1	6.5	1	0.028	0. 044	0.044

and CO, and ratios for gas synthesis (H_2/CO) were calculated from Equations (5)-(9).

$$CH_4\ Conversion\% = \frac{(CH_4)_{in} - (CH_4)_{out}}{(CH_4)_{in}} \times 100 \quad (5)$$

$$CO_2\ Conversion\% = \frac{(CO_2)_{in} - (CO_2)_{out}}{(CO_2)_{in}} \times 100 \quad (6)$$

$$H_2\ Selectivity\% = \frac{H_2}{2\left[(CH_4)_{in} - (CH_4)_{out}\right]} \times 100 \quad (7)$$

$$CO\ Selectivity\% = \frac{CO}{\left[(CH_4)_{in} - (CH_4)_{out}\right] + \left[(CO_2)_{in} - (CO_2)_{out}\right]} \times 100 \quad (8)$$

$$H_2/CO\ ratio = \frac{H_2\ Selectivity\%}{CO\ Selectivity\%} \quad (9)$$

3. Results and Discussion

3.1 Physicochemical Characterizations of Catalyst

3.1.1 X-ray Diffraction (XRD) Method

Figure 1(a-d) illustrates the XRD patterns of the catalysts with different calcium and lanthanum contents. The diffraction peaks recorded at 2θ = 23.1°, 29.3°, 35.8°, 39.3°, 43.1°, 47.5°, 48.5°, and 64.7° were due to the cubic form of calcium oxide (JCPDS file no.: 00-017-0912). Meanwhile, the diffraction peaks recorded at 2θ = 27.2°, 31.5°, and 44.9° were due to the cubic form of Lanthanum oxide (JCPDS file no.: 00-004-0856). The peaks recorded at 2θ = 15.6°, and 62.2° were attributed to the cubic form of the catalyst complex (La-Ca-O). However, in all the patterns, there were no diffraction peaks for the catalyst with 1% cobalt, nickel, and palladium, due to the minimum amount of the elements. This observation concurs with the results reported by Grange [20]. The Debye-

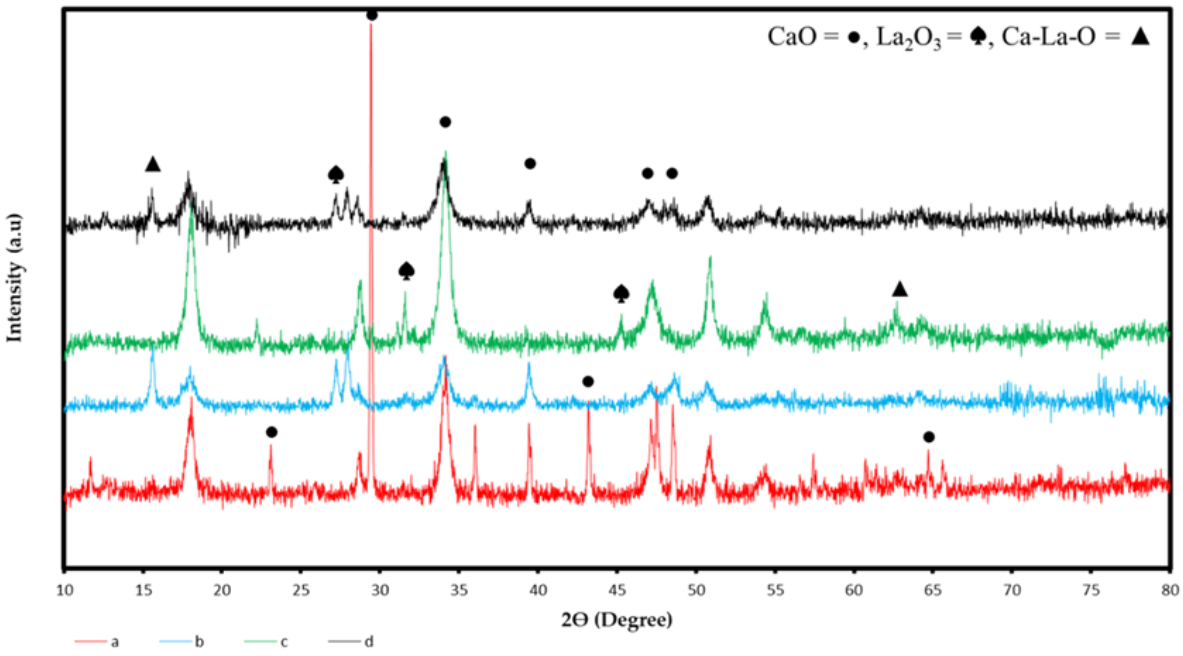

Figure 1. XRD patterns of the catalysts: (a) Co,Ni,Pd/CaO, (b) Co,Ni,Pd/$Ca_{0.97}La^{3+}_{0.03}O$, (c) Co,Ni,Pd/$Ca_{0.93}La^{3+}_{0.07}O$, (d) Co,Ni,Pd/$Ca_{0.85}La^{3+}_{0.15}O$.

Table 2. Particle size measurement by XRD, TEM, and XRF results.

Catalysts	TEM (nm)	Crystal size (D) Debye-Sherrer equation (nm)	XRF			
			Ni%	Pd%	Co%	CaO & La%
Co,Ni,Pd/CaO	47.5	40.5	0.79	0.89	0.93	96.38
Co,Ni,Pd/$Ca_{0.97}La^{3+}_{0.03}O$	53.3	43.8	0.85	0.76	0.69	96.66
Co,Ni,Pd/$Ca_{0.93}La^{3+}_{0.07}O$	40.3	38.7	0.89	0.81	0.65	95.95
Co,Ni,Pd/$Ca_{0.85}La^{3+}_{0.15}O$	36.4	37.6	0.92	0.83	0.88	96.62

Scherrer's equation was used to calculate the crystal size of the Catalysts through the diffraction of the highest peak in the XRD patterns. The crystal size was observed at 40.5, 43.8, 38.7, and 37.6 nm for the following catalysts of Co,Ni,Pd/CaO, Co,Ni,Pd/$Ca_{0.97}La^{3+}_{0.03}O$, Co,Ni,Pd/$Ca_{0.93}La^{3+}_{0.07}O$, and Co,Ni,Pd/$Ca_{0.85}La^{3+}_{0.15}O$ catalysts, respectively. The results depicted that the amount of Lanthanum was inversely related to crystal size. As the amount of Lanthanum increased, the crystal size decreased. This happened due to the outgrowth of calcium crystallites due to the effects of the residue of Co, Ni, and Pd on the sample surface. The XRD findings revealed a cubic crystal structure for all the samples, further backed by the TEM findings that also showed cubic-shaped particles. XRF has been used for the elemental analysis of all the components in the catalyst. Table 2 shows the percentage of Co, Ni, and Pd [21].

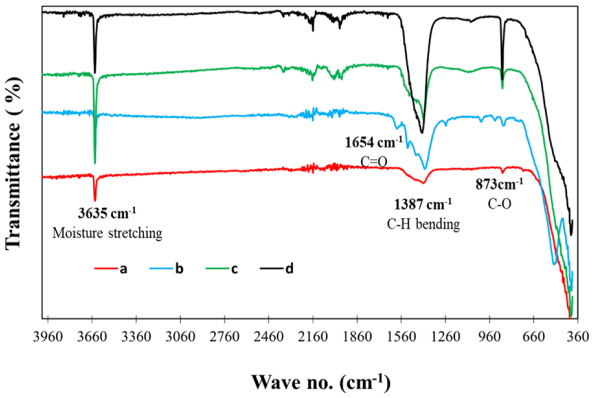

Figure 2. FT-IR Spectra of the catalysts: (a) Co,Ni,Pd/CaO, (b) Co,Ni,Pd/$Ca_{0.97}La^{3+}_{0.03}O$, (c) Co,Ni,Pd/$Ca_{0.93}La^{3+}_{0.07}O$, (d) Co,Ni,Pd/$Ca_{0.85}La^{3+}_{0.15}O$.

3.1.2 FT-IR Method

Figure 2 shows FT-IR data for the catalysts of Co,Ni,Pd/CaO, Co,Ni,Pd/$Ca_{0.97}La^{3+}_{0.03}O$, Co,Ni,Pd/$Ca_{0.93}La^{3+}_{0.07}O$, and Co,Ni,Pd/$Ca_{0.85}La^{3+}_{0.15}O$ were prepared through the impregnation of Co,Ni,Pd(acac)$_2$ on the CaO-La_2O_3. The spectra of the unreduced catalysts indicated bands in the region of (3637-480 cm^{-1}) which were characteristic of acetylacetonate ligands. The bands recorded at 1654 and 1506 cm^{-1} in the FTIR were assigned to the presence of C=O and C=C bonds of acetylacetonate in the primary catalyst (Co,Ni,Pd(acac)$_2$) complex [22]. The band at 3050 cm^{-1} and 1387 cm^{-1} can be assigned to the existence of C−H stretching and bending, respectively. Figure 2 demonstrates the other

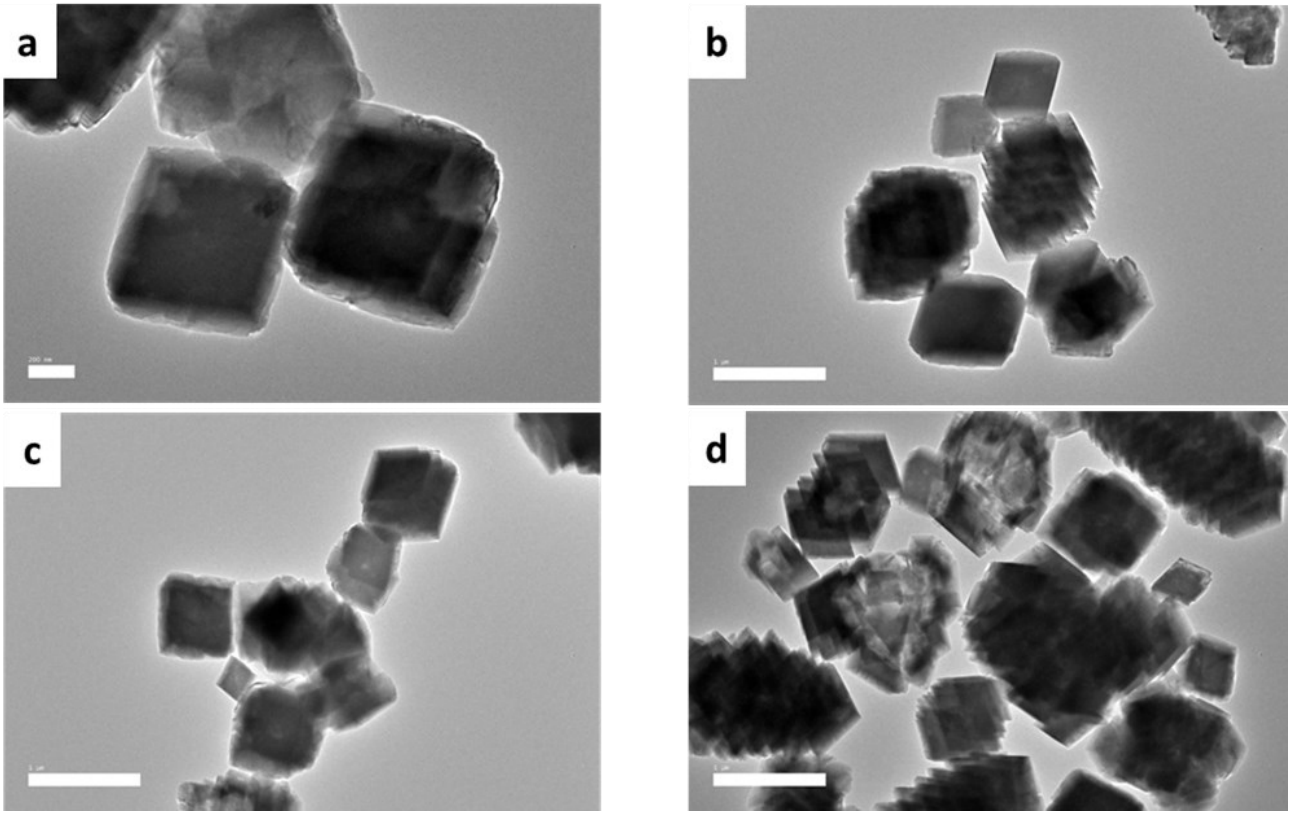

Figure 3. TEM image of catalysts: (a) Co,Ni,Pd/CaO, (b) Co,Ni,Pd/$Ca_{0.97}La^{3+}_{0.03}O$, (c) Co,Ni,Pd/$Ca_{0.93}La^{3+}_{0.07}O$, (d) Co,Ni,Pd/$Ca_{0.85}La^{3+}_{0.15}O$.

bands in the spectra which showed the presence of acetylacetonate. The band at 831-873 cm^{-1} corresponded to the C–O bond, while the peak at 480, 685, and 775 cm^{-1} corresponded to NiO, CoO, and PdO, respectively [23,24], as per the reported data. A band at around 3635-3637 cm^{-1} was attributed to the stretching frequency of moisture [25]. The peaks for CaO and LaO did not appear in the spectra due to their presence in the far FTIR range.

3.1.3 TEM Method

Figure 3(a-d) illustrates the TEM images of the catalysts Co,Ni,Pd/CaO, $Co,Ni,Pd/Ca_{0.97}La^{3+}{}_{0.03}O$, $Co,Ni,Pd/Ca_{0.93}La^{3+}{}_{0.07}O$, and $Co,Ni,Pd/Ca_{0.85}La^{3+}{}_{0.15}O$ with cubic structures. The conditions used for these catalysts were calcination at 1150 °C with a uniform particle distribution without free La_2O_3. Figure 3(b-d) confirmed the formation of the CaO-La_2O_3 solid solutions [26], with cubic oxide particles on the Co, Ni, and Pd layers of the supported metal. The size of catalyst particles on the support Ca-La ranged from 45 to 85 nm [27]. The TEM analysis of the catalyst, $Co,Ni,Pd/Ca_{0.85}La^{3+}{}_{0.15}O$, indicated that an accumulation of the nanoparticles at a specific distance between the metal crystallites induces growth. In general, metallic cobalt, nickel, and palladium catalyze this type of growth. Although the size distribution obtained from the images of TEM was more realistic and accurate, the size distribution presented some limitations. $Co,Ni,Pd/Ca_{0.97}La^{3+}{}_{0.03}O$ (Figure 3(b)) was well dispersed with 1% of the Co, Ni, and Pd metal.

3.1.4 BET Surface Area and Pore Analysis

Table 3 lists the surface areas obtained from BET analysis of samples, pore volume, and pore radius of the $Co,Ni,Pd/Ca_{1-x}La_xO$ catalysts: (where x = 0.00, 0.03, 0.07, and 0.15). The surface area of catalysts Co,Ni,Pd/CaO with a cubic structure supported with TEM was 12.3 m^2/g, while the surface area for the support CaO was 12.1 m^2/g. The highest reading for the former was due to the loading of Co, Ni, and Pd on the specific surface area of the support CaO. In this case, the surface areas of the catalysts Co,Ni,Pd/CaO were considerably lower than the surface areas of the conventional catalysts: $Co,Ni,Pd/Ca_{0.97}La^{3+}{}_{0.03}O$ $Co,Ni,Pd/Ca_{0.93}La^{3+}{}_{0.07}O$, and $Co,Ni,Pd/Ca_{0.85}La_{3+0.15}O$, which were recorded at 13.0, 12.4 and 16.3 m^2/g, respectively. This happens because Calcium oxide pores were partially covered by the layer of Co, Ni, and Pd particles. However, the BET surface area of the CaO, which La_2O_3 promoted, was almost similar to conventional catalysts Co, Ni, and Pd with binary support [28]. Besides, the characteristics of the supported Co, Ni, and Pd catalysts with a cubic structure included extremely low metal dispersion, small surface areas of the Co, Ni, and a few Pd particles. This could possibly be due to the strong interaction between the Co, Ni, and Pd layers and the support of CaO with the promoter La_2O_3. The pore volume showed inter-particle gaps due to the pore size of the catalyst, $Co,Ni,Pd/Ca_{0.85}La_{3+0.15}O$, was recorded at 0.075 cm^3/g. This value was slightly more significant than the value of the other catalysts, which was recorded at 0.21 cm^3/g. This differs from the study of Bao *et al.* [29]. Table 3, shows the pore radius of the different catalysts. The pore radius of the support CaO was recorded at 9.9 Å, whereas the pore radius of the catalyst Co,Ni,Pd/CaO was recorded at 15.4 Å. The pore radius of the remaining catalysts was inversely proportionate to the increase in support of the promoter, La_2O_3, whereby the pore radius of the catalysts, they are: $Co,Ni,Pd/Ca_{0.97}La^{3+}{}_{0.03}O$, $Co,Ni,Pd/Ca_{0.93}La^{3+}{}_{0.07}O$, and $Co,Ni,Pd/Ca_{0.85}La^{3+}{}_{0.15}O$ were recorded at 24.7 Å, 24.8 Å, and 86.6 Å, respectively [30]. This illustrates that the catalyst $Co,Ni,Pd/Ca_{0.85}La_{3+0.15}O$ with a high surface area performed better in the dry reforming of the methane reaction than the other catalysts.

3.1.5 H_2-TPR Method

The H_2-TPR experiments were conducted on the following catalysts: Co,Ni,Pd/CaO,

Table 3. The main textural properties of fresh catalysts.

Sample name	Specific surface are (m^2/g)	Pore volume (cm^3/g)	Pore radius (Å)
CaO	12.1	0.22	9.9
Co,Ni,Pd/CaO	12.3	0.020	15.4
$Co,Ni,Pd/Ca_{0.97}La^{3+}{}_{0.03}O$	13.0	0.028	24.7
$Co,Ni,Pd/Ca_{0.93}La^{3+}{}_{0.07}O$	12.4	0.030	24.8
$Co,Ni,Pd/Ca_{0.85}La^{3+}{}_{0.15}O$	16.3	0.075	86.6

$Co,Ni,Pd/Ca_{0.97}La^{3+}_{0.03}O$, $Co,Ni,Pd/Ca_{0.93}La^{3+}_{0.07}O$, and $Co,Ni,Pd/Ca_{0.85}La^{3+}_{0.15}O$ to investigate their reduction behaviour. Figure 4(a-d) and Table 4 illustrate the H_2-TPR profiles of these catalysts. Figure 4(a) shows three well-defined reduction peaks in the H_2-TPR profile of Co,Ni,Pd/CaO. The first reduction peak was recorded at 360 °C. This was attributed to the reduction of the CoO species in the production of Co, as compared to the previous study [31]. The second reduction peak was positioned at 161 °C, due to the reduction of PdO to Pd. The third and fourth peaks were at the region of 540 and 580 °C, associated with the reduction of NiO on the surface and in the bulk of the catalyst respectively, indicating a strong interaction with the supporting material [29]. Figure 4(b-d) and Table 4 illustrate the H_2-TPR profile for the catalysts, including the promoter La_2O_3. The H_2-TPR profiles for $Co,Ni,Pd/Ca_{0.97}La^{3+}_{0.03}O$, $Co,Ni,Pd/Ca_{0.93}La^{3+}_{0.07}O$, and $Co,Ni,Pd/Ca_{0.85}La^{3+}_{0.15}O$ catalysts were quite different from the catalyst Co,Ni,Pd/CaO. These findings showed five peaks. The first four peaks of the catalyst $Co,Ni,Pd/Ca_{0.97}La^{3+}_{0.03}O$ were recorded at 386 °C, 202 °C, 556 °C and 582 °C, while the peaks of the catalyst of $Co,Ni,Pd/Ca_{0.93}La^{3+}_{0.07}O$ were recorded at 315 °C, 135 °C, 527 °C, and 587 °C. The peaks of the catalyst of $Co,Ni,Pd/Ca_{0.85}La^{3+}_{0.15}O$ were observed at 377 °C, 150 °C, 540 °C, and 634 °C. This was due to the reduction of CoO, PdO, and NiO on the surface and the bulk of the catalysts to obtain the elements Co°, Ni°, and Pd°, respectively. The fifth peak of the following synthesized catalysts of $Co,Ni,Pd/Ca_{0.97}La^{3+}_{0.03}O$, $Co,Ni,Pd/Ca_{0.93}La^{3+}_{0.07}O$, and $Co,Ni,Pd/Ca_{0.85}La^{3+}_{0.15}O$ was found at temperatures 670 °C, 626 °C, and 695 °C, respectively, corresponding to the reduction of La_2O_3 on the surface. There was a significant lowering of the surface of La_2O_3 when there was a reduction in the temperature of the catalyst. Various possible explanations for this phenomenon have been put forward. One possible reason could be a significant improvement in the dispersion of La_2O_3 particles during the incorporation of CaO into La_2O_3 in the matrix and the impeding of sintering [32].

Another reason could be due to the strong interaction between La_2O_3 and Co, Pd, and Ni metals during the overlapping of the CoO, NiO,

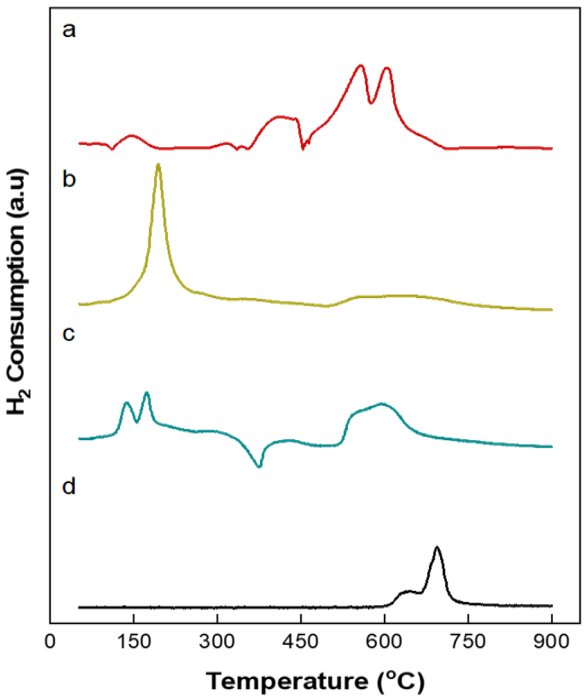

Figure 4. H_2-TPR profiles of catalysts: (a) Co,Ni,Pd/CaO, (b) $Co,Ni,Pd/Ca_{0.97}La^{3+}_{0.03}O$, (c) $Co,Ni,Pd/Ca_{0.93}La^{3+}_{0.07}O$, (d) $Co,Ni,Pd/Ca_{0.85}La^{3+}_{0.15}O$ reduced in a (5% H_2/Ar) stream at a temperature ramp of 10 °C/min.

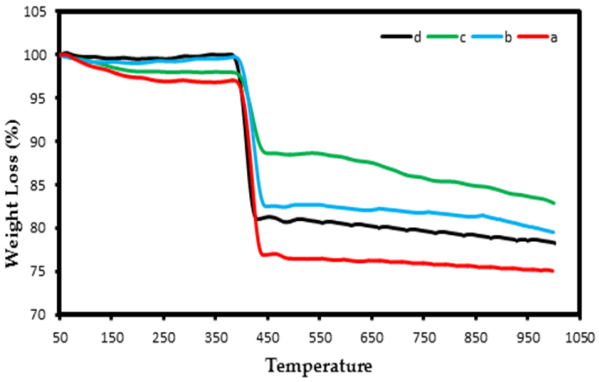

Figure 5. TG of the catalysts: (a) Co,Ni,Pd/CaO, (b) $Co,Ni,Pd/Ca_{0.97}La^{3+}_{0.03}O$, (c) $Co,Ni,Pd/Ca_{0.93}La^{3+}_{0.07}O$, (d) $Co,Ni,Pd/Ca_{0.85}La^{3+}_{0.15}O$.

Table 4. H_2-TPR results of the different catalysts.

Catalysts	Temperature (°C)					Amount of Adsorbed H_2 gas (μmol/g)
Co,Ni,Pd/CaO	360	161	540	580	-	597.9
$Co,Ni,Pd/Ca_{0.97}La^{3+}_{0.03}O$	386	202	556	582	670	842.0
$Co,Ni,Pd/Ca_{0.93}La^{3+}_{0.07}O$	315	135	527	587	626	516.2
$Co,Ni,Pd/Ca_{0.85}La^{3+}_{0.15}O$	377	150	540	634	695	944.3

PdO, and La_2O_3, resulting in the reduction of peaks [33]. It is also evident that adding the promoter, La_2O_3, effectively reduces catalysts, potential with CaO support. This could be attributed to the basic properties of the support. It has been found that $Ca_{1-x}La^{3+}{}_xO$ with higher basicity than CaO interacts more with the La_2O_3 promoter. Thus, the reductions in CoO, NiO, and PdO are attributed to the redox property of $Ca_{1-x}La^{3+}{}_xO$ [34].

The total amount of H_2-consumption in the reduction of Co,Ni,Pd/CaO, $Co,Ni,Pd/Ca_{0.97}La^{3+}{}_{0.03}O$, $Co,Ni,Pd/Ca_{0.93}La^{3+}{}_{0.07}O$, and $Co,Ni,Pd/Ca_{0.85}La^{3+}{}_{0.15}O$ was calculated from the total area of the peaks. The calculations for the catalysts were 597.9, 842.0, 516.2, and 944.3 μmol/g catalyst, respectively. The H_2-TPR results indicated that the catalyst $Co,Ni,Pd/Ca_{0.85}La^{3+}{}_{0.15}O$ was the most active site among the other catalysts. In other words, it is the best catalyst for the dry reforming of methane in this study.

3.1.6 TGA Method

Figure 5(a-d) shows the analysis of the TGA for the reduced catalysts, Co,Ni,Pd/CaO, $Co,Ni,Pd/Ca_{0.97}La^{3+}{}_{0.03}O$, $Co,Ni,Pd/Ca_{0.93}La^{3+}{}_{0.07}O$, and $Co,Ni,Pd/Ca_{0.85}La^{3+}{}_{0.15}O$. These findings indicate a weight loss at only a certain stage of the thermal process. The practical weight loss was recorded at about 23.3%, 15.2%, 12.5% and 17.7% for the catalysts (a-d), respectively, at temperatures ranging from 400 °C to 435 °C. which might be associated with the removal of acetylacetone group from the $Co,Ni,Pd/Ca_{1-x}La_xO$ catalysts. At 600 °C, all the samples stayed stable due to the high melting point of calcium oxide and La_2O_3 at 2572 and 2315 °C, respectively. From Figure 5(a-d), the catalyst components interacted well. These results are similar to those of Al-Najar *et al.* [32].

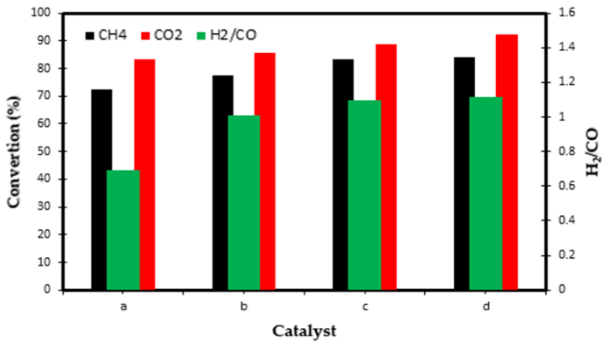

Figure 6. The effect of using different catalysts (a) Co,Ni,Pd/CaO, (b) $Co,Ni,Pd/Ca_{0.97}La^{3+}{}_{0.03}O$, (c) $Co,Ni,Pd/Ca_{0.93}La^{3+}{}_{0.07}O$, and (d) $Co,Ni,Pd/Ca_{0.85}La^{3+}{}_{0.15}O$, on CH_4, CO_2 conversion and H_2/CO ratio at 900 °C for the 1:1 ratio of CH_4:CO_2.

3.2 Catalytic Performance in Biogas Reforming

3.2.1 Effect of the catalyst concentration on conversion

Figure 6 displays the impact of the concentration of the catalyst during the conversion process. The conversion of CH_4, CO_2, and the ratio of H_2/CO were in ascending order as in Co,Ni,Pd/CaO < $Co,Ni,Pd/Ca_{0.97}La^{3+}{}_{0.03}O$ < $Co,Ni,Pd/Ca_{0.93}La^{3+}{}_{0.07}O$ < $Co,Ni,Pd/Ca_{0.85}La^{3+}{}_{0.15}O$. The Co and Pd were combined with nickel on the support, CaO-La_2O_3. The studies were carried out under the following conditions: a temperature of 900 °C and 1 atm with a feed ratio (CH_4:CO_2) of (1:1). Regarding the conversion of methane, the catalyst $Co,Ni,Pd/Ca_{0.85}La^{3+}{}_{0.15}O$ had the maximum conversion (84%); while the catalyst Co,Ni,Pd/CaO had the lowest conversion (72%). Overall, the conversion of CO_2 was more stable than methane, and the catalyst $Co,Ni,Pd/Ca_{0.85}La^{3+}{}_{0.15}O$ had the highest conversion of CO_2 (92%), while the catalyst Co,Ni, Pd/CaO had the lowest conversion (83%).

In all the tri-metallic CaO-La_2O_3 catalysts, as shown in Figure 6, the product ratio of H_2/CO was more than 1. This indicated that in contrast to the other research [29], the Ni metal's CO_2 conversion process was less advantageous than the tri-metallic catalysts. The conversion rates of CH_4 and CO_2, as well as the ratio of H_2/CO, increased when lanthanum oxide's concentration increased, as shown in Figure 6. The catalyst $Co,Ni,Pd/Ca_{0.85}La^{3+}{}_{0.15}O$ showed exceptional performance, attributed to its most active site in the H_2-TPR and the ex-

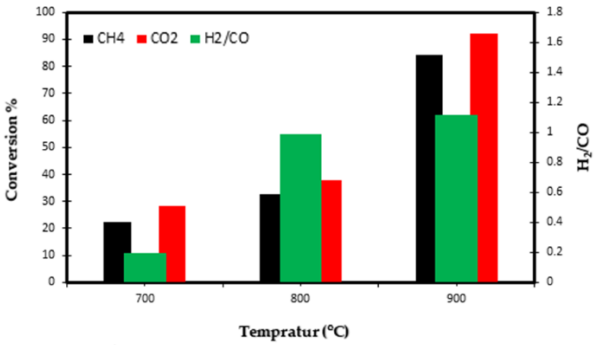

Figure 7. The influence of temperature on the catalytic activity of the $Co,Ni,Pd/Ca_{0.85}La^{3+}{}_{0.15}O$ catalyst: (1) 700 °C, (2) 800 °C, (3) 900 °C for the 1:1 ratio of CH_4:CO_2.

tensive surface area revealed by the BET analysis. This suggests that the addition of La_2O_3 to CaO catalysts can notably inhibit the Reverse Water Gas Shift (RWGS) reaction (Equation (10)).

$$CO_2 + H_2 \rightarrow CO + H_2O \quad (10)$$
$$\Delta H_{298\,K} = 41 \text{ kJ mol}^{-1}$$

3.2.2 Effects of temperature on conversion

Figure 7 displays the activity and selectivity results of the catalyst Co,Ni,Pd/$Ca_{0.85}La^{3+}_{0.15}O$ at a temperature range of 700 to 900 °C. Generally, the conversion of CH_4:CO_2 (1:1) increased when the temperature was raised from 700 °C to 900 °C, owing to the solid endothermic reaction of dry reforming (Equation (1)).

According to earlier studies, the conversion rate increases at a higher temperature [35]. It is noted that when there was an increase in temperature from 700 °C to 900 °C, the CH_4 conversion of Co,Ni,Pd/$Ca_{0.85}La^{3+}_{0.15}O$ displayed an increase from 22% to 84%, with a rise in the CO_2 conversion from 28% to 92%. However, there was no discernible increase in the CH_4 and CO_2 conversion rates when the temperature was above 900 °C. The H_2/CO ratio of the catalyst at various temperatures is shown in Figure 7. The H_2/CO ratio of the samples was less than 1 when the temperature was below 900 °C. The H_2/CO ratio may decrease as a result of the reverse water-gas-shift reaction (RWGS) (Equation (10)), which has the potential to consume the additional H_2 and produce CO. The H_2/CO ratio of Co,Ni,Pd/$Ca_{0.85}La^{3+}_{0.15}O$ was measured at 1.11 at 900 °C, indicating a negligible contribution from the RWGS reaction (Equation (10)) [36].

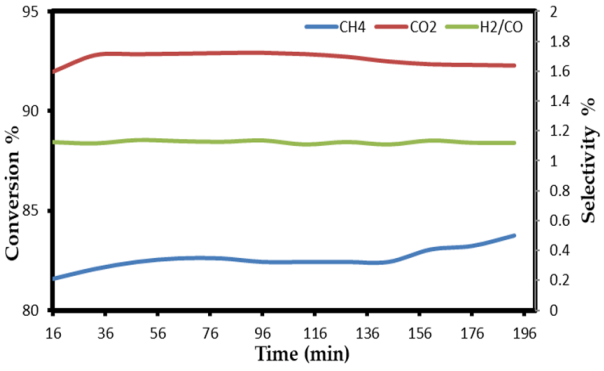

Figure 8. Stability tests of Co,Ni,Pd/$Ca_{0.85}La^{3+}_{0.15}O$ catalysts at 900 °C for the 1:1 ratio of CH_4:CO_2 for 5 h. (GHSV = 15000 mL.gc_{at}^{-1}.h^{-1}, atmospheric pressure).

Table 4 presents a summary of the results obtained by comparing the performance of the catalyst chosen in this study with other supported catalysts reported in recent publications. The usage of well-chosen support and promoter in catalyst proves to be highly beneficial, enhancing catalytic performance and promoting synergistic interactions that contribute to superior activity and selectivity. Furthermore, above moderate CO_2 and CH_4 conversion rates of 54-92% with H_2/CO ratio in the range of 0.45-1 have been reported. This conversion rate and H_2/CO ratio are influenced by various parameters such as the type of supports and promoters used, feed gas ratio, and reaction temperature. Among the investigated catalysts, the Co,Ni,Pd/$Ca_{0.85}La^{3+}_{0.15}O$ catalyst, synthesized and evaluated in this study, stands out with exceptional results. Operating under a feed ratio of CH_4:CO_2 at 1:1 and a reaction temperature of 900 °C, the catalyst achieves a CH_4 and CO_2 conversion rate of 84% and 92% respectively. The incorporation of La_2O_3 into the CaO support emerges as a key contributing factor, effectively inhibiting the Reverse Water Gas Shift (RWGS) reaction. Therefore, the developed Co,Ni,Pd/$Ca_{0.85}La^{3+}_{0.15}O$ catalyst in this research holds great potential for the dry reforming of methane process.

Table 5. Catalytic activity for dry reforming of methane reaction using different catalysts.

Catalysts	Reaction conditions		Conversion (%)		H_2/CO ratio	Ref.
	Feed ratio CH_4/CO_2	Temperature (°C)	CH_4	CO_2		
La-NiCu/SiO_2	1:1	750	55.2	89	-	[37]
Ni/La_2O_3	1:1	700	70	75	0.87	[38]
10Ni/SBA-15	1:1	700	54	62	0.64	[39]
Ni/MoCeZr/$MgAl_2O_4$-MgO	1:1	800	85	84	0.87	[40]
5%Ni-10%Co/Al_2O_3	1:1	700	67	71	~1	[41]
Y_2O_3-Co/Mesoporous Al_2O_3	1:1	900	88	95	0.45	[42]
Co,Ni,Pd/$Ca_{0.85}La^{3+}_{0.15}O$	1:1	900	84	92	1.11	This work

3.2.3 Stability tests

Figure 8 shows the reading of the temperature tests. The findings revealed that when the temperature was at 900 °C, the conversion for both CH_4 and CO_2 was high. The activity and stability of the tri-metallic catalyst Co, Ni, and Pd were much higher than that of the mono-metallic catalyst Ni or bi-metallic catalysts Pd-Ni and Co-Ni. This concurs with the assumption that Co and Pd help prevent the oxidation of Ni due to an increase in its electron density [43]. When there is a high concentration of La_2O_3, the conversion rate of CH_4 and CO_2 decreases, but when there is a decrease in the concentration of lanthanum oxide, it indicates that CO_2 is being converted through the active formation of substantial ionic oxides like $La_2O_3.CO_3$ attracts CO_2 to the top catalyst layer and thus increases the conversion rate of CH_4. A reduction in the concentration of La_2O_3 may result from the high electron density of Co, Ni, and Pd [36]. The La_2O_3-supported catalysts facilitated the adsorption of carbon dioxide. The lanthanum adsorption improves the dispersion stability of tiny mineral particles and its promotional effect on CO_2. In essence, lanthanum is an oxide that has been demonstrated to react vigorously during the supporting process of metals. Both oxides and metals have seen notable changes in their surface properties [37]. It was discovered that mono-metallic catalysts, such as Ni or Pd, and bimetallic catalysts, like Co and Ni, were less stable and less active than three-metal catalysts, such as Co, Ni, and Pd with excellent results as shown in Table 5 and Figure 6. This can be because, as previously discussed, Co and Pd are trying to transfer the electronic density to the metal Ni, which serves as the primary catalyst in the triple catalyst. The notion that Nickel metals are oxidized by Co and Pd, increasing the electron density, is consistent with this data [43,44]. When the bi-metallic Co-Ni or Pd-Ni cluster is created, Ni's reducibility rises. Such circumstances increase the reliability of laboratory operations beyond 5 h [26,45].

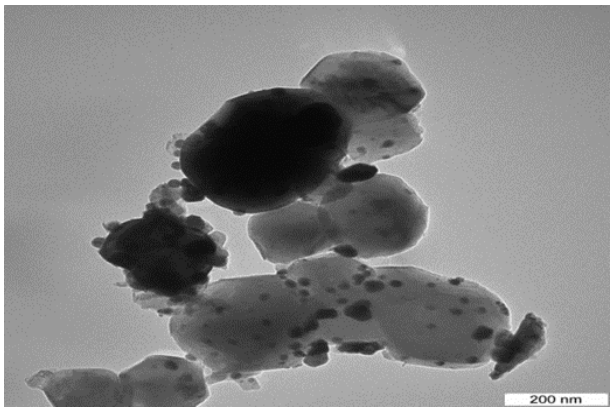

Figure 9. TEM image of $Co,Ni,Pd/Ca_{0.85}La^{3+}{}_{0.15}O$ catalyst after 5 h reaction, at 900 °C, and CH_4/CO_2 ratio 1:1.

3.2.4 Post-reaction characterization

Figure 9 illustrates the TEM findings for the spent catalyst which revealed an additional carbon layer without any filamentous carbon presence. The amount of coke deposited on the spent catalyst was calculated to be 1.5%wt. In summary, the data indicates minimal coke accumulation on the catalysts, suggesting that coke formation might be influenced by the catalysts' metal dispersion. Also, the metal catalysts with smaller crystal sizes were more resistant to deactivation, aligning with observations made Al-Doghachi *et al.* [19].

4. Conclusion

Tri-metallic catalysts $Co,Ni,Pd/Ca_{1-x}La_xO$, with varying Ca to La molar ratios, were developed using the co-precipitation method, employing K_2CO_3 as the precipitator. The catalysts' physical and chemical properties were analyzed using XRD, XRF, FT-IR, H_2-TPR, BET, TEM, and TGA. These synthesized catalysts were then tested in the DRM reaction, with the $Co,Ni,Pd/Ca_{0.85}La^{3+}{}_{0.15}O$ catalyst exhibiting the highest catalytic efficiency at 900 °C. Furthermore, the catalyst showed commendable stability during the 5 h test, obtaining a conversion of 92% for CO_2 and 84% for CH_4. Moreover, XRD and H_2-TPR analysis further revealed that the $Co,Ni,Pd/Ca_{0.85}La^{3+}{}_{0.15}O$ catalyst possessed a smaller active metal particle size and a more uniform dispersion than other catalysts. Notably, a Co-Ni-Pd alloy structure on this catalyst enhanced the metal-support interaction, promoting its catalytic performance and stability.

CRediT Author Statement

Faris A.J. Al-Doghachi: Conceptualization, Validation, Data curation and Writing – original draft preparation. Ali M.A. Al-Najar: Software, Methodology,Formal analysis, Investigation, Writing - Original Draft; M. Safa-Gamal: Formal analysis; Yun Hin Taufiq-Yap: Supervision, Resources, Funding acquisition.

References

[1] Taufiq-Yap, Y.H., Al-Doghachi, F.A. (2018). CO_2 reforming of methane over Ni/MgO catalysts promoted with Zr and La oxides. *ChemistrySelect*, 3(2), 816-827. DOI: 10.1002/slct.201701883.

[2] le Saché, E., Santos, J., Smith, T., Centeno, M., Arellano, H., Odriozola, J., Reina, T. (2018). Multicomponent Ni-CeO_2 nanocatalysts for syngas production from CO_2/CH_4 mixtures. *Journal of CO2 Utilization*, 25, 68-78. DOI: 10.1016/j.jcou.2018.03.012.

[3] Stroud, T., Smith, T., Saché, L., Santos, J., Centeno, M., Arellano, H., Odriozola, J., Reina, T. (2018). Chemical CO_2 recycling via dry and bi reforming of methane using Ni-Sn/Al_2O_3 and Ni-Sn/CeO_2-Al_2O_3 catalysts. *Applied Catalysis B: Environmental*, 224, 125-135. DOI: 10.1016/j.apcatb.2017.10.047.

[4] Acharya, K., Al-Fatesh, A.S., Almutairi, G., Fakeeha, A.H., Ibrahim, A.A., Abasaeed, A.E., Kumar, R. (2023). The Role of Strontium as an Economic Promoter Over WO^{3+}-ZrO_2 Supported Ni Catalyst for H_2 Production through Dry Reforming of Methane. *Catalysis Letters*, 1-13. DOI: 10.1007/s10562-023-04450-8.

[5] Al-Doghachi, F.A.J., Murad, D.M., Al-Niaeem, H.S., Al-Jaberi, S.H., Mohamad, S., Taufiq-Yap, Y.H. (2021). High Active Co/$Mg_{1-x}Ce_x^{3+}O$ Catalyst: Effects of Metal-Support Promoter Interactions on CO_2 Reforming of CH_4 Reaction. *Bulletin of Chemical Reaction Engineering & Catalysis*, 16(1), 97-110. DOI: 10.9767/bcrec.16.1.9969.97-110.

[6] Dębek, R., Motak, M., Grzybek, T., Galvez, M., Da Costa, P. (2017). A short review on the catalytic activity of hydrotalcite-derived materials for dry reforming methane. *Catalysts*, 7, 32. DOI: 10.3390/catal7010032.

[7] Hambali, H., Jalil, A., Abdulrasheed, A., Siang, J., Gambo, Y., Umar, A., (2022). Zeolite and clay based catalysts for CO_2 reforming of methane to syngas: a review. *International Journal of Hydrogen Energy*, 47(72), 30759-30787. DOI: 10.1016/j.ijhydene.2021.12.214.

[8] Taherian, Z., Gharahshiran, V.S., Orooji, Y., Karimi-Maleh, H., Khataee, A. (2023). The study of CO_2 reforming of methane over Ce/Sm-promoted NiCaAl catalysts. *Process Safety and Environmental Protection*, 174, 235-242. DOI: 10.1016/j.psep.2023.03.046.

[9] Schwengber, C., da Silva, F., Schaffner, R., Fernandes, N., Ferracin, R., Bach, V., Alves, H. (2016). Methane dry reforming using Ni/Al_2O_3 catalysts: evaluation of the effects of temperature, space velocity and reaction time. *Journal of Environmental Chemical Engineering*, 4(3), 3688-3695. DOI: 10.1016/j.jece.2016.07.001.

[10] Wang, J., Fan, G., Li, F. (2012). Carbon-supported Ni catalysts with enhanced metal dispersion and catalytic performance for hydrochlorination of chlorobenzene. *RSC Advances*, 2, 9976-9985. DOI: 10.1039/C2RA21216A.

[11] Al-Doghachi, F.A., Jassim, A.F., Taufiq-Yap, Y.H. (2020). Enhancement of CO_2 Reforming of CH_4 Reaction Using Ni,Pd,Pt/$Mg_{1-x}Ce_x^{4+}O$ and Ni/$Mg_{1-x}Ce_x^{4+}O$ Catalysts. *Catalysts*, 10(11), 1240. DOI: 10.3390/catal10111240.

[12] Álvarez Moreno, A., Ramirez-Reina, T., Ivanova, S., Roger, A.C., Centeno, M.Á. and Odriozola, J.A. (2021). Bimetallic Ni–Ru and Ni–Re catalysts for dry reforming of methane: Understanding the synergies of the selected promoters. *Frontiers in Chemistry*, 9, 694976. DOI: 10.3389%2Ffchem.2021.694976.

[13] Zhang, X., Zhang, L.H., You, X., Peng, C.X., Liu, W., Fang, X., Wang, Z., Zhang, N., Wang, X. (2018). Nickel nanoparticles embedded in mesopores of AlSBA-15 with a perfect peasecod-like structure: a catalyst with superior sintering resistance and hydrothermal stability for dry methane reforming. *Applied Catalysis B: Environmental*, 224, 488-499. DOI: 10.1016/j.apcatb.2017.11.001.

[14] Liu, W., Li, L., Zhang, X., Wang, Z., Wang, X., Peng, H. (2018). Design of Ni-ZrO_2-SiO_2 catalyst with ultra-high sintering and coking resistance for dry reforming of methane to prepare syngas. *Journal of CO2 Utilization*, 27, 297-307. DOI: 10.1016/j.jcou.2018.08.003.

[15] Peng, H., Zhang, X., Han, X., You, X., Lin, S., Chen, H., Liu, W., Wang, X., Zhang, N., Wang, Z., Wu, P., Zhu, H., Dai, S. (2019). Catalysts in coronas: a surface spatial confinement strategy for high-performance catalysts in dry methane reforming. *ACS Catalysis*, 9, 9072-9080. DOI: 10.1021/acscatal.9b00968.

[16] Nazemi, M., Sheibani, S., Rashchi, F., Gonzalez-DelaCruz, V., Caballero, A. (2012). Preparation of nanostructured nickel aluminate spinel powder from spent NiO/Al_2O_3 catalyst by mechanochemical synthesis. *Advanced Powder Technology*, 23, 833-838. DOI: 10.1016/j.apt.2011.11.004.

[17] Yuan, X., Li, B., Wang, X., Li, B. (2022). Synthesis gas production by dry reforming of methane over Neodymium-modified hydrotalcite-derived nickel catalysts. *Fuel Processing Technology*, 227, 107104. DOI: 10.1016/j.fuproc.2021.107104.

[18] lvarez, A., Ramirez, T., Ivanova, S., Roger, A., Centeno, M., Odriozola, J.A. (2021). Bimetallic Ni-Ru and Ni–Re catalysts for dry reforming of methane: Understanding the synergies of the selected promoters. *Frontiers in Chemistry*, 9, 694976. DOI: 10.3389%2Ffchem.2021.694976.

[19] Al-Doghachi, F.A., Rashid, U., Taufiq-Yap, Y. H. (2016). Investigation of Ce (III) promoter effects on the tri-metallic Pt,Pd,Ni/MgO catalyst in dry-reforming of methane. *RSC advances*, 6(13), 10372-10384. DOI: 10.1039/C5RA25869C.

[20] Law, Z.X., Pan, Y.T., Tsai, D.H. (2022). Calcium looping of CO_2 capture coupled to syngas production using Ni-CaO-based dual functional material. *Fuel*, 328, 125202. DOI: 10.1016/j.fuel.2022.125202.

[21] Oyama, S., Hacarlioglu, P., Gu, Y., Lee, D. (2012). Dry reforming of methane has no future for hydrogen production: comparison with steam reforming at high pressure in standard and membrane reactors. *International Journal of Hydrogen Energy*, 37, 10444-10450. DOI: 10.1016/j.ijhydene.2011.09.149.

[22] Al-Doghachi, F.A., Rashid, U., Zainal, Z., Saiman, M.I., Taufiq-Yap, Y.H. (2015). Influence of Ce_2O_3 and CeO_2 promoters on Pd/MgO catalysts in the dry-reforming of methane. *RSC Advances*, 5(99), 81739-81752. DOI: 10.1039/C5RA15825G.

[23] Ahmad, Y., Mohamed, A., Kumar, A., Al-Qaradawi, S. (2021). Solution combustion synthesis of Ni/La_2O_3 for dry reforming of methane: tuning the basicity via alkali and alkaline earth metal oxide promoters. *RSC Advances*, 11(53), 33734-33743. DOI: 10.1039%2Fd1ra05511a.

[24] Hossain, M.A., Ayodele, B.V., Cheng, C.K., Khan, M.R. (2018). Syngas production from catalytic CO_2 reforming of CH_4 over $CaFe_2O_4$ supported Ni and Co catalysts: full factorial design screening. *Bulletin of Chemical Reaction Engineering & Catalysis*, 13(1), 57-73. DOI: 10.9767/bcrec.13.1.1197.57-73.

[25] Devaraja, P., Avadhani, D., Prashant, S., Nagabhushana, H., Sharma, S., Nagabhushana, B., Nagaswarupa, H. (2014). Synthesis, structural and luminescence studies of magnesium oxide nanopowder. *Spectrochimica Acta Part A: Molecular and Biomolecular Spectroscopy*, 4, 810-834. DOI: 10.1016/j.saa.2013.08.050.

[26] Messaoudi, H., Thomas, S., Slyemi, S., Djaidja, A., Barama, A. (2020). Syngas production via methane dry reforming over La-Ni-Co and La-Ni-Cu catalysts with spinel and perovskite structures. *Bulletin of Chemical Reaction Engineering & Catalysis*, 15(3), 885-897. DOI: 10.9767/bcrec.15.3.9295.885-897.

[27] Kim, H., Kang, K., Kwak, H. (2009). Preparation of supported Ni catalysts with a core/shell structure and their catalytic tests of partial oxidation of methane, *International Journal of Hydrogen Energy*, 34, 3351-3359. DOI: 10.1016/j.ijhydene.2009.02.036.

[28] Sandoval-Diaz, L.E., Schlögl, R., Lunkenbein, T. (2022). Quo vadis dry reforming of Methane? A review on its chemical, environmental, and industrial prospects. *Catalysts*, 12(5), 465. DOI: 10.3390/catal12050465.

[29] Bao, Z., Lu, Y., Han, J., Li, Y., Yu, F. (2015). Highly Active and Stable Ni-based Bimodal Pore Catalyst for Dry Reforming of Methane. *Applied Catalysis A: General*, 491, 116-126. DOI: 10.1016/j.apcata.2014.12.005.

[30] Ahmed, W., Awadallah, A., Aboul, E. (2016). Ni/CeO_2-Al_2O_3 Catalysts for Methane Thermo-catalytic Decomposition to CO_x-free H_2 Production. *International Journal of Hydrogen Energy*, 41, 18484-18493. DOI: 10.1016/j.ijhydene.2016.08.177.

[31] James, O., Maity, S. (2016). Temperature programmed reduction (TPR) studies of cobalt phases in γ-alumina supported cobalt catalysts. *Journal of Petroleum Technology and Alternative Fuels*, 7, 1-12. DOI: 10.5897/JPTAF2015.0122.

[32] Al-Najar, A.M., Al-Doghachi, F.A., Al-Riyahee, A.A., Taufiq-Yap, Y.H. (2020). Effect of La_2O_3 as a promoter on the Pt, Pd, Ni/MgO catalyst in dry reforming of methane reaction. *Catalysts*, 10(7), 750. DOI: 10.3390/catal10070750.

[33] Gonzalez-Delacruz, V., Ternero, F., Pereñíguez, R., Caballero, A. (2010). Study of nanostructured Ni/CeO_2 catalysts prepared by combustion synthesis in dry reforming of methane. *Applied Catalysis A: General*, 384, 1-9. DOI: 10.1016/j.apcata.2010.05.027.

[34] Slimani, R., El Ouahabi, I., Abidi, F. (2014). Calcined eggshells as a new bio sorbent to remove basic dye from aqueous solutions: thermodynamics, kinetics, isotherms, and error analysis. *Journal of the Taiwan Institute of Chemical Engineers*, 45(4), 1578-1587. DOI: 10.1016/j.jtice.2013.10.009.

[35] Appari, S., Janardhanan, V.M., Bauri, R., Jayanti, S., Deutschmann, O. (2014). Detailed kinetic model for biogas steam reforming on Ni and catalyst deactivation due to sulfur poisoning. *Applied Catalysis A: General*, 471, 118-125. DOI: 10.1016/j.apcata.2013.12.002.

[36] Kehres, J., Jakobsen, J., Andreasen, J., Wagner, J., Liu, H., Molenbroek, A., Vegge, T. (2012). Dynamical Properties of a Ru/$MgAl_2O_4$ Catalyst During Reduction and Dry Methane Reforming. *The Journal of Physical Chemistry C*, 116, 21407-21415. DOI: 10.1021/jp3069656.

[37] Meng, Z., Wang, Z. (2021). The Effect of Different Promoters (La_2O_3, CeO_2, and ZrO_2) on the Catalytic Activity of the Modified Vermiculite-Based Bimetallic NiCu/EXVTM-SiO_2 Catalyst in Methane Dry Reforming. *ACS Omega*, 6(44), 29651-29658. DOI: 10.1021/acsomega.1c03959.

[38] Li, X., Li, D., Tian, H., Zeng, L., Zhao, Z.-J., Gong, J. (2017). Dry reforming of methane over Ni/La_2O_3 nanorod catalysts with stabilized Ni nanoparticles. *Applied Catalysis B: Environmental*, 202, 683–694. DOI: 10.1016/j.apcatb.2016.09.071.

[39] Taherian, Z., Yousefpour, M., Tajally, M. and Khoshandam, B. (2017). Catalytic performance of Samaria-promoted Ni and Co/SBA-15 catalysts for dry reforming of methane. *International Journal of Hydrogen Energy*, 42(39), 24811–24822. DOI: 10.1016/j.ijhydene.2017.08.080.

[40] Huang, Y., Li, X., Zhang, Q., Vinokurov, V.A., Huang, W. (2022). Carbon deposition behaviours in dry reforming of CH_4 at elevated pressures over Ni/MoCeZr/$MgAl_2O_4$-MgO catalysts. *Fuel*, 310, 122449. DOI: 10.1016/j.fuel.2021.122449.

[41] Siang, T.J., Singh, S., Omoregbe, O., Bach, L.G., Phuc, N.H.H., Vo, D.V.N. (2018). Hydrogen production from CH_4 dry reforming over bimetallic Ni–Co/Al_2O_3 catalyst. *Journal of the Energy Institute*, 91(5), 683–694. DOI: 10.1016/j.joei.2017.06.001.

[42] Mohd Jailani, M.S.A., Miskan, S.N., Bahari, M.B., Setiabudi, H.D. (2023). Optimization of dry reforming of methane over Yttrium Oxide-Cobalt/Mesoporous alumina using response surface methodology. *Materials Today: Proceedings,* In Press. DOI: 10.1016/j.matpr.2023.04.690.

[43] Steinhauer, B., Kasireddy, M., Radnik, J., Martin, A. (2009). Development of Ni-Pd Bimetallic Catalysts for the Utilization of Carbon Dioxide and Methane by Dry Reforming. *Applied Catalysis A: General*, 366, 333-341. DOI: 10.1016/j.apcata.2009.07.021.

[44] Istadi, I., Anggoro, D., Amin, N., Ling, D. (2011). Catalyst deactivation simulation through carbon deposition in carbon dioxide reforming over Ni/CaO-Al_2O_3 catalyst, *Bulletin of Chemical Reaction Engineering & Catalysis*, 6, 129-136. DOI: 10.9767/bcrec.6.2.1213.129-136.

[45] Miguel, S., Vilella, I., Maina, S., Alonso, D.J., Martinez, M.R., Gomez, I.M. (2012). Influence of Pt addition to Ni catalysts on the catalytic performance for long term dry reforming of methane. *Applied Catalysis A: General*, 435, 10-18. DOI: 10.1016/j.apcata.2012.05.030.